PCCP

The initiation of traveling pulses from self-organized oscillations in the iron–nitric acid system

Konstantin Agladze,† Stephanie Thouvenel-Romans and Oliver Steinbock*

Florida State University, Department of Chemistry, Tallahassee, FL 32306-4390, USA

Received 24th November 2000, Accepted 6th February 2001
First published as an Advance Article on the web 2nd March 2001

The spatio–temporal dynamics of dissolution patterns on low-carbon steel wires submerged in nitric acid solution are studied in an electrolytic cell by means of optical detection. The cathodic steel wire can segregate into different macroscopic domains. With increasing distance from the external anode, these domains are characterized by constant dissolution, rapidly pulsating oscillations, excitable behavior, and constant passivity. For nitric acid concentrations between 10.5 M and 12.0 M, the fast oscillations trigger traveling waves that experience propagation failures far from the anode. The rhythm of successful wave generation is typically slower and less regular than the rhythm of the rapid oscillations.

Introduction

Decades of research have revealed that the vast majority of electrochemical reactions can undergo dynamic instabilities.[1–4] Under appropriate conditions these instabilities induce bistable behavior,[5] oscillations,[6] intermittency[7] and different flavors of chaos.[7–9] However, the self-organization of electrochemical systems is not limited to temporal phenomena but can also involve spatial pattern formation. Standing and propagating waves have been observed in a variety of dissolution reactions of metals such as cobalt[10] and nickel[11] as well as in the electrocatalytic oxidation of formic acid on platinum ring electrodes.[12,13] Furthermore, waves were detected by surface plasmon microscopy on silver ring electrodes during the reduction of peroxodisulfate.[14]

The classic example for spatio–temporal pattern formation in electrochemistry is the dissolution of iron. It is well known that iron as well as certain other metals and alloys show the phenomenon of metallic passivity.[1,2] That is, iron becomes essentially inert under particular environmental conditions (*e.g.*, appropriate acidity) since its surface is covered by a thin oxide film. Metallic passivity can be characterized in terms of the corresponding N-shaped polarization curve.[15,16] For the case of iron in acidic solution, one observes a rise in dissolution rate with increasing electrode potential (active state). At the passivation (or Flade) potential, the dissolution rate is drastically reduced and the metal surface becomes passivated. Under these conditions, the system forms an excitable medium in which the passive state is a stable but excitable attractor. At even higher values of the electrode potential, the dissolution rate increases again and the system shifts into the transpassive state.

In the passive state defects of the protective film can induce propagating reaction zones in which the leading activation front is often accompanied by a trailing repassivation transition that recovers the protective surface film.[17–22] Here, the spatial coupling is predominantly mediated by electric currents[1,2] and may be considered a local one if the potential distribution generated by an anodic defect or wave does not appreciably widen into the system.[2] An important parameter that controls the coupling range is the electrode arrangement.[2] In addition, phenomena due to thermal conductivity, surface tension or convection can contribute to the overall dynamics.

Propagating waves of excitation are frequently found in spatially extended, non-linear systems.[23] Important examples are oxidation waves in the Belousov–Zhabotinsky reaction[24,25] and propagating nerve impulses[26] that arise from diffusion coupling and local-current coupling, respectively. Furthermore, excitation-like waves have been observed in the iron–nitric acid system under open-circuit conditions.[27] A remarkable example is the existence of rotating spiral waves on low-carbon steel plates.[28]

The work presented here provides experimental data on the spatio–temporal self-organization of the iron–nitric acid system. We analyze the potential-dependent dynamics of this system by unfolding it spatially along steel wires that are subjected to an applied electric field. Furthermore, we demonstrate the formation of localized oscillations which can serve as intricate initiation sites of propagating activation and passivation fronts.

Experimental

The experimental set-up consists of a low-carbon steel wire (Malin Co.; ~0.07% C, <0.4% Mn, <0.04% P, <0.05% S) and a platinum electrode submerged in nitric acid solution. The diameter of the steel wire is 2.0 mm. The concentration of nitric acid (Fisher) is varied between 10 M and 15 M and the height of the solution (volume: 180 ml) is kept constant at 6.5 mm. The platinum electrode is used as an external anode and is placed 8 mm from one end of the steel wire in extension of the wire's direction. The steel wire itself serves as the cathode in the electrolytic cell. It should be noted that the height of the electrolyte can influence the dynamics of the system, if the thickness of the solution is decreased to values below approximately 5 mm. Possible sources for this dependence are the local currents in the electrolyte, the hydrodynamic flow patterns and/or the transport of oxygen from the gas phase into the system.

The solution and the electrodes were kept on ice at 0 °C to reduce the influence of chemical and ohmic heat production as well as to slow down the dynamics of the system for ease of detection. In the absence of an externally applied potential, neither dissolution fronts nor oscillations are observed.

† On leave from: Institute of Theoretical and Experimental Biophysics, Pushchino, Moscow Region 142292, Russia.

 DOI: 10.1039/b009425k

However, the dissolution reaction can be initiated by applying an appropriate electric potential. The reaction zone is clearly visible as a dark brownish area, while passivated regions have a grayish color.

The spatio–temporal behavior of the system is monitored with a monochrome charged-coupled-device (CCD) camera. The spatial resolution of this optical detection method is high compared to the one of classical strategies that employ arrays of electrodes. The optical signal, however, is less quantitative in nature and has also a lower signal-to-noise ratio. The video signals are digitized using a PC-based frame grabber board (Data Translation; 640 × 480 pixels resolution with 8 bit pixel^{-1}) and stored on a hard disk for further processing. The video frames are captured with a sampling rate of 3.3 frames s^{-1}. The image data allow the extraction of time–space plots. In this analysis, each snapshot of a sequence was scanned along the wire yielding the local gray level as a function of the wire's arclength. The time–space plot is then generated by piling up subsequent, one-dimensional intensity profiles in the vertical direction. Consequently, a wave that propagates along the wire will be represented in the time–space plot as a black band. The slopes of the boundaries of this band are inversely proportional to the velocities of the activation and repassivation front.

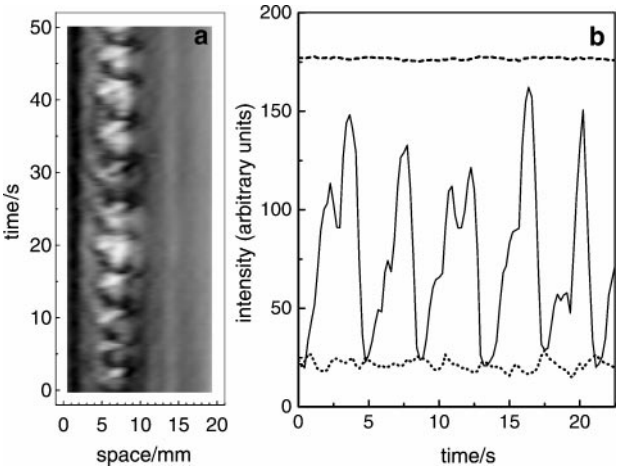

Fig. 1 Spatio–temporal dynamics along a low-carbon steel wire at $[HNO_3] = 13.5$ M. The cathodic wire shows three distinct domains in which the system undergoes continuous dissolution, oscillations, and passivity. (a) Time–space plot: Bright and dark areas correspond to passive and active regions, respectively. (b) Time-series of the image intensity in these three regions: The dashed, solid and dotted curves are obtained by calculating the temporal evolution of the spatial intensity average from the regions $x < 1$ mm (active), 5.4 mm $< x <$ 6.5 mm (oscillatory) and 22 mm $< x <$ 32 mm (passive), respectively.

Results

In the absence of an externally applied potential, the steel wire is uniformly passivated. However, the dissolution reaction can be induced by applying a voltage that exceeds a critical threshold value. Under the given experimental conditions, this critical value increases with increasing acidity from approximately 0.25 V to 0.5 V and is closely related to the pH-dependent passivation potential and the conductivity of the electrolyte. If the applied potential is supercritical, a brownish region forms at the end of the steel wire located closest to the anode. The brownish color results from the removal of the passivation film and the continuous electrodissolution of iron, which is accompanied by the formation of rust particles. In the following, we will describe the spatio–temporal behavior of the system for different concentrations of nitric acid.

Fig. 1a shows a time–space plot of a steel wire submerged in 13.5 M nitric acid. The illustrated behavior is typical for systems at high concentrations of nitric acid. The platinum anode is located at $x = -8$ mm (not shown). The left-hand side of the time–space plot shows a dark, vertical stripe. This stripe corresponds to a zone of continuous dissolution and has a width of approximately 2–3 mm. Adjacent to this zone we found a second region in which the surface of the metal oscillates rapidly between the active and passive state. This oscillatory region is typically larger (here 7 mm) than the one of continuous dissolution. Adjacent to the oscillatory zone the steel is uniformly passivated ($x > 10$ mm).

The dynamics of the three different regions is also illustrated in Fig. 1b which shows the temporal evolution of the gray levels detected in these regions. These optical data are obtained by calculating the average gray levels within the three domains from the time–space plot in Fig. 1a. High and low intensities correspond to the passive and active state of the metal surface, respectively. Under the given experimental conditions, the period of the electrochemical oscillations is (4.5 ± 1) s.

A similar behavior is found for slightly lower concentrations of nitric acid. The time–space plots in Fig. 2a,b represent typical experiments at $[HNO_3] = 12.6$ M and 12.2 M, respectively. They show the same patterning of the cathode into three distinct areas. The continuously active and the oscillatory area, however, expand in width as the acidity of the system is decreased. This finding is also illustrated in Fig. 2c. The intensity data, $I(x,t)$, compiled in the time–space plots allow the extraction of the function, $I_x(t)$, for all positions, x, along the steel wire. Each of these intensity series fluctuates around its temporal average, I_x, with an amplitude that is large in the oscillatory region but negligibly small in the continuously activated and passive areas. The statistical variance, $\sigma^2(x)$, of the local time series is a convenient measure for this dependence. Fig. 2c shows the normalized variance, $\sigma^2(x)/\mathrm{Max}(\sigma^2(x))$, as a function of the position along the cathode for three different concentrations of nitric acid. For each concentration, we found one interval of high variance which corresponds to the oscillatory region. The analysis confirms the visual impression that the oscillatory region expands with decreasing acidity. Notice that also the distance between the oscillatory region and the anode increases with decreasing concentration of nitric acid.

Fig. 2a,b reveal an additional feature of the observed electrochemical oscillations. The duration of the passive phase seems to increase with increasing distance from the continuously active region. In the time–space plots, this position-dependent shape of the oscillations generates structures that are reminiscent of horizontal "icicles". In the experiment, it creates the impression of breathing fronts that periodically originate at and return to the active zone.

The features of the passive region of the steel wire change dramatically if the concentration of nitric acid is decreased to 12 M or smaller. Under these conditions, long-range pulses nucleate in the oscillatory region and propagate towards the far end of the wire. Fig. 3 shows two typical examples observed at $[HNO_3] = 10.5$ M and 11.5 M. The magnification of the time–space plots in Fig. 3 is approximately ten times smaller than the one used in Fig. 2. The high temporal resolution of the data shown in Fig. 3a reveals that the duration of the dissolution pulse decreases in the course of propagation. This phenomenon creates the dark, saw-tooth-like structures in the time–space plot (Fig. 3a) and arises from a significant difference between the velocity of the activation and the repassivation transition. The propagation velocity of the activation front varies in the range 1–2 cm s^{-1}. The repassivation front, however, is so much faster that no reliable data could be obtained. It remains, therefore, unclear whether the repassivation transition is indeed an actively propagating front or a local event that is solely controlled by the temporal kinetics of the electrodissolution process. At higher concentra-

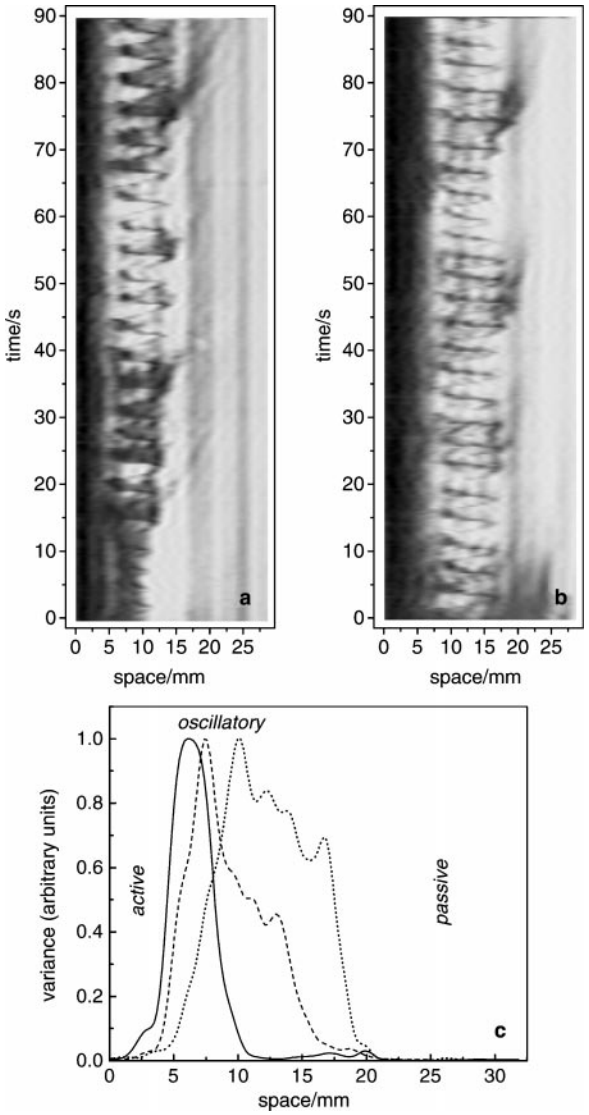

Fig. 2 Time–space plots obtained from experiments with $[HNO_3]$ = 12.6 M (a) and 12.2 M (b). The intensity data in a given time–space plot allow the calculation of the variance, $\sigma^2(x) \propto \sum_t (I(x,t) - \bar{I}(x))^2$, at any position, x, along the cathode. The variance is a measure of the amplitude of the local intensity changes around the corresponding temporal average, $\bar{I}(x)$. The curves in (c) show the normalized variance as a function of position along the steel wire. The solid, dashed and dotted lines are obtained for $[HNO_3]$ = 13.5 M, 12.6 M and 12.2 M, respectively. The oscillatory domains can be identified as regions of high variance. The width of the active and the oscillatory region increases with decreasing concentration of nitric acid.

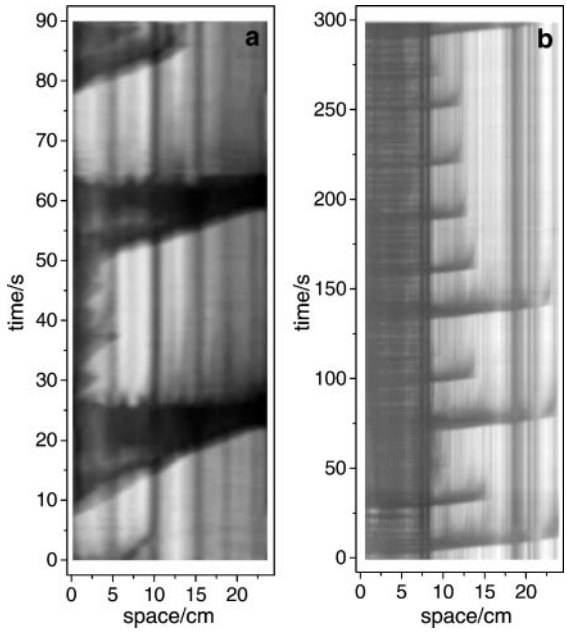

Fig. 3 Time–space plots of the electrochemical patterns along the steel wire for low concentrations of nitric acid. Under these conditions, the oscillatory region emits propagating pulses into the passive area of the cathode. The vertical stripes are artifacts that arise from inhomogeneous reflection of light from the curved steel surface. Concentration of nitric acid: 10.5 M (a) and 11.5 M (b).

tions of nitric acid, the continuous decrease of the duration of the dissolution pulse can induce propagation failures. Fig. 3b represents such an experiment in which only three out of ten waves succeed in propagating along the full length of the steel wire. There is no unique position at which the propagation failures occur and there appears to be an intricate dependence between the lifetime of the pulses and the history of the system.

Fig. 3 also illustrates that the period of the pulses is significantly longer than the period of the localized oscillations. This relative increase in period stems from the initially very long duration of pulses and possibly from slow recovery processes that are either hidden from or not resolved in our experiments.

The pulse nucleation depicted in Fig. 3 is reminiscent of phenomena observed in externally forced excitable systems such as the Belousov–Zhabotinsky reaction.[29,30] The response of these excitable systems to fast periodic perturbations can follow complex Farey sequences[30] of successful and unsuccessful trigger events. The firing number of a particular sequence is defined as the fraction between the number of trigger events and perturbations within a complete cycle of the entire system. In our experiments, this scenario is complicated by the spatial character of the system, the presence of slow transients in the system, and possibly by undesired stochastic perturbations that arise from the formation of gas bubbles and rust particles. However, the presented example is unique in the sense that the periodic pacemaker is generated by a constant external perturbation (*i.e.*, the applied potential) and that this self-organized pacemaker gives rise to surprisingly small firing numbers.

The periodicity of the fast, localized oscillations depends only slightly on the concentration of nitric acid. Fig. 4 shows the period of these fast oscillations for acid concentrations between 10.5 M and 14.5 M. The average oscillation period (square symbols) is approximately 5 s with the longest period being detected at $[HNO_3]$ = 14.5 M. As mentioned above, we observed propagating pulses only for concentrations of nitric acid up to 12 M. The time between successive long-range pulses shows significant fluctuations (compare Fig. 3b). In a given experiment, it can vary by a factor of two or more. The open triangles in Fig. 4 summarize the corresponding experimental data for different concentrations of nitric acid. The time between successive pulses decreases with decreasing acidity and the rhythm of successful initiation events becomes more regular. At $[HNO_3]$ = 10.5 M the traveling pulses extend over the entire wire and seem to coincide with the breathing oscillations.

All of the above measurements are carried out at the minimal voltage required for induction of fast oscillations. This critical potential increases with the concentration of nitric acid (Table 1) as well as with the distance between anode and cathode (here always 8 mm). Fig. 5 shows two time–space plots that illustrate the dynamics of the iron–nitric acid system at different above-threshold values of the applied

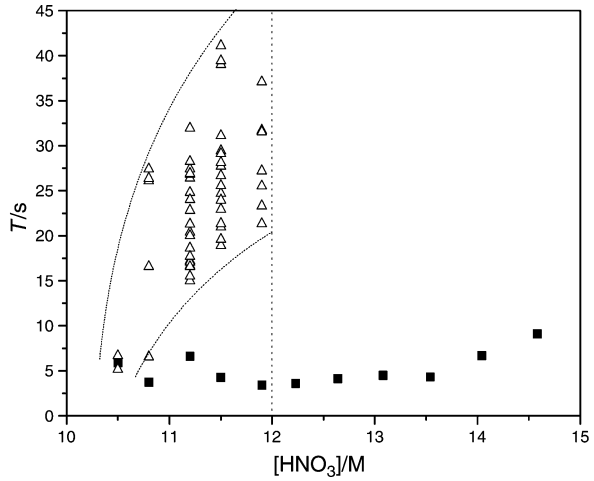

Fig. 4 Elapsed time, T, between successive activation events for different concentrations of nitric acid. The solid squares indicate the period of the fast, breathing oscillations. The open triangles represent data obtained from propagating pulses. The time delays between successive pulses fall into a funnel-shaped region of the diagram. No pulses were observed for concentrations of nitric acid above approximately 12 M (vertical dashed line).

potential. The response of the cathode to an increase in the applied potential is qualitatively similar to its response against a decrease in nitric acid concentration. For example, at the high concentration of $[HNO_3] = 11.9$ M, we observed that an increase in the potential from 0.6 V to 0.8 V leads to a pronounced expansion of the continuously active area (Fig. 5a,b).

Table 1 Dependence of the critical potential, E_{crit}, on the concentration of nitric acid. For subcritical potentials, the cathode remains uniformly passive and no oscillations are observed

$[HNO_3]$/M	E_{crit}/V
10.5	0.28
11.2	0.30
11.8	0.35
12.2	0.39
12.6	0.43
13.1	0.48

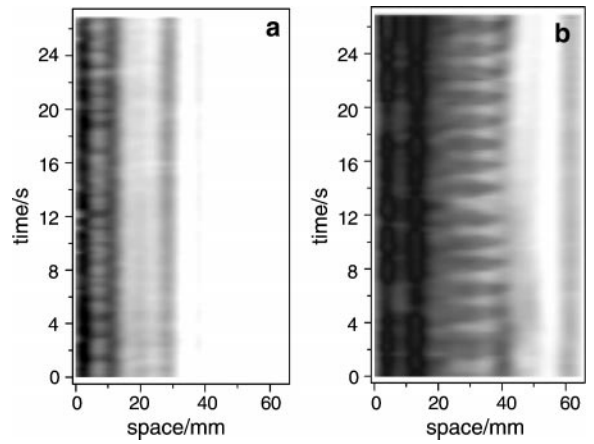

Fig. 5 Time–space plots of the iron–nitric acid system obtained for different values of the externally applied potential: (a) 0.6 V and (b) 0.8 V. Both experiments were carried out at $[HNO_3] = 12$ M (*i.e.*, slightly above the critical concentration for pulse initiation).

Also the length of the oscillatory region increases with the applied potential and the breathing character of the oscillations becomes more distinct. Furthermore, at approximately 1.0 V and higher, we observed the formation of frequent long-range pulses that propagate into the passive region of the steel wire.

Discussion

The potential-dependent active and oscillatory regions as well as the critical potential are intimately related to the potential distribution in the experimental system. Their existence can be motivated from a simple static picture which disregards the impedance and the capacitance of the system. The potential drop through the surface film of the uniformly passivated steel is determined by resistance of the film, which remains essentially constant along the passivated wire. The IR drop within the electrolyte, however, depends on the distance, l, between the anode and the point of interest on the cathode, the conductivity of the electrolyte and the geometry of the electrolytic cell (Fig. 6).[2,31] Since the geometry of the system was not changed in our experiments, one can associate the IR drop with an effective resistance $R_E(l)$ that depends on the distance, l, in a monotonically increasing fashion. The potential difference across the surface film decays monotonically with l and increases with the externally applied potential. If the potential difference is sufficiently strong, the system can shift from the passive into the active state and the dissolution reaction of iron is initiated. Since $R_E(l)$ increases monotonically for increasing values of l, one expects to observe continuous dissolution in a region of the cathode that is located closest to the anode. The quantitative dependence of R_E on l, however, is complex since it reflects the specific geometry of the electrolytic cell (for more information on this problem see refs. 2 and 32). In addition, a more realistic description of the observed phenomena will have to involve the impedance and the capacitance of the surface film.

Based on the above qualitative argument, it is possible to interpret our experimental findings as follows: Under the given conditions, the externally applied potential unfolds the temporal dynamics of the iron–nitric system along the cathodic wire. Accordingly, we observe a permanently active state in the region closest to the anode. Adjacent to this region the system is shifted to an oscillatory state that sweeps through the parameter space as we depart from the anode. However, the range of possible oscillation modes and periods is strongly altered by the spatial coupling of neighboring segments and induces the fast, breathing oscillations reported in this study. The next nearest domain appears to be an excitable state that allows the propagation of either sustained or damped pulses. In our experiments, the propagating pulses are always triggered by the fast oscillations. Even farther away from the anode, the IR drop has become so significant that the potential drop at the film is not sufficient to destabilize the

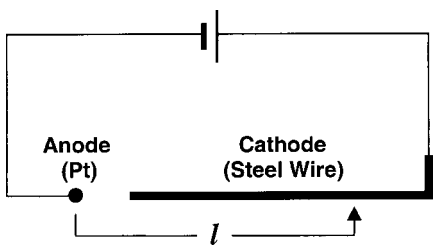

Fig. 6 Schematic representation of the electrolytic cell. The variable, l, denotes the distance between the anode and given points on the cathode.

passive state of the system. This region has no clear demarcation on the cathode but extends towards the far end of the steel wire. The lack of a clear demarcation is reflected in the variable positions at which propagation failures occur and probably arises from slow recovery processes that control the formation of the final passivation film. These processes are also the source of the small firing numbers observed in our experiments. It should be noted that this detailed analysis has been made possible by the use of optical detection techniques that, if applicable supply data of high spatial resolution.

At concentrations of nitric acid slightly below 10.5 M, the system appears to be truly excitable even in the absence of an applied potential. Earlier studies, carried out by electrochemical means of detection and slightly different experimental parameters, indicate that these conditions seem to allow the propagation of the dissolution pulse over very long and possibly infinite distances.[20] Under our experimental conditions, however, this concentration range was not suitable for controlled experiments since the exothermicity of the overall reaction led to a rapid increase in temperature and to pronounced gas formation.

The presented study emphasizes the importance of the geometry of the electrolytic cell and the relative placement of the involved electrodes since both factors can influence the global characteristics of the system in an unexpected fashion. These factors are of profound relevance because they are inherent in electrochemical measurements and in corrosion protection systems. Most importantly, however, our experiments provide an example for the spatial unfolding of the potential-dependent bifurcation structure of a passive metal, which is accompanied by an intricate initiation sequence of pulses that undergo subsequent propagation failures. Therefore, this study should also provide an interesting test case for numerical simulations of pattern formation in electrochemical systems.[33–36]

Acknowledgement

This work was financially supported by the Florida State University.

References

1 J. L. Hudson and T. T. Tsotsis, *Chem. Eng. Sci.*, 1994, **49**, 1493.
2 K. Krischer, in *Modern Aspects of Electrochemistry, Number 32*, ed. B. E. Conway, J. O'M. Bockris and R. E. White, Kluwer, New York, 1999, pp. 1–142.
3 M. T. M. Koper, *Electrochim. Acta*, 1992, **37**, 1771.
4 M. T. M. Koper, *J. Chem. Soc., Faraday Trans.*, 1998, **94**, 1369.
5 G. Flätgen, K. Krischer and G. Ertl, *Z. Naturforsch., A: Phys. Sci.*, 1995, **50**, 1097.
6 J. L. Hudson and M. R. Bassett, in *Reviews in Chemical Engineering*, ed. D. Luss and N. R. Amundson, Freund, London, 1991.
7 M. R. Bassett and J. L. Hudson, *Chem. Eng. Commun.*, 1987, **60**, 145.
8 M. R. Bassett and J. L. Hudson, *J. Phys. Chem.*, 1989, **93**, 2731.
9 I. Z. Kiss, W. Wang and J. L. Hudson, *Phys. Chem. Chem. Phys.*, 2000, **2**, 3847.
10 R. D. Otterstedt, P. J. Plath, N. I. Jaeger and J. L. Hudson, *J. Chem. Soc., Faraday Trans.*, 1996, **92**, 2933.
11 O. Lev, M. Sheintuch, L. M. Pismen and C. Yarnitzky, *Nature*, 1988, **336**, 488.
12 J. Christoph, P. Strasser, M. Eiswirth and G. Ertl, *Science*, 1999, **284**, 291.
13 P. Strasser, J. Christoph, W. F. Lin and J. L. Hudson, *J. Phys. Chem. A*, 2000, **104**, 1854.
14 G. Flätgen, K. Krischer, B. Pettinger, K. Doblhofer, H. Junkes and G. Ertl, *Science*, 1995, **269**, 668.
15 H. Kaesche, *Die Korrosion der Metalle*, Springer, Berlin, 1990.
16 K. J. Vetter, *Electrochemical Kinetics*, Academic Press, New York, 1967.
17 R. S. Lillie, *J. Gen. Physiol.*, 1925, **7**, 473.
18 K. F. Bonhoeffer, *J. Gen. Physiol.*, 1948, **32**, 69.
19 U. F. Franck, *Z. Elektrochem.*, 1958, **62**, 649.
20 R. Suzuki, *Adv. Biophys.*, 1976, **9**, 115.
21 J. L. Hudson, J. Tabora, K. Krischer and I. G. Kevrekidis, *Phys. Lett. A*, 1993, **179**, 355.
22 S. F. Nassar, H. A. Ismail, E. M. Sayed and A. El-Falaky, *Appl. Phys.*, 1975, **7**, 307.
23 A. G. Merzhanov and E. N. Rumanov, *Rev. Mod. Phys.*, 1999, **71**, 1173.
24 A. T. Winfree, *Science*, 1972, **175**, 634.
25 N. Manz, S. C. Müller and O. Steinbock, *J. Phys. Chem. A*, 2000, **104**, 5895.
26 A. L. Hodgkin and A. F. Huxley, *J. Physiol. (London)*, 1952, **117**, 500.
27 G. Horanyi, G. Inzelt and E. Szetey, *Acta Chim. Hung.*, 1978, **97**, 299.
28 K. Agladze and O. Steinbock, *J. Phys. Chem. A*, 2000, **104**, 9816.
29 S. K. Scott, *Chemical Chaos*, Oxford University Press, Oxford, 1991.
30 Á. Tóth, V. Gaspar and K. Showalter, *J. Phys. Chem.*, 1994, **98**, 522.
31 G. Flätgen and K. Krischer, *J. Chem. Phys.*, 1995, **103**, 5428.
32 N. Mazouz, G. Flätgen and K. Krischer, *Phys. Rev. E: Stat. Phys., Plasmas, Fluids, Relat. Interdiscip. Top.*, 1997, **55**, 2260.
33 U. F. Franck and R. FitzHugh, *Z. Elektrochem.*, 1961, **65**, 156.
34 M. T. M. Koper and J. H. Sluyters, *J. Electroanal. Chem.*, 1993, **347**, 31.
35 M. T. M. Koper and J. H. Sluyters, *Electrochim. Acta*, 1993, **38**, 1535.
36 A. Birzu, B. J. Green, R. D. Otterstedt, N. I. Jaeger and J. L. Hudson, *Phys. Chem. Chem. Phys.*, 2000, **2**, 2715.